The Impact of Temperature and Switching Rate on Dynamic Transients of High Voltage Silicon and 4H-SiC NPN BJTs: A Technology Evaluation

Saeed Jahdi *Member, IEEE,*, Mohammad Hedayati, Bernard H. Stark, and Phil H. Mellor

***Abstract*—This paper reports the application of silicon BJT modelling techniques to the modelling of dynamic behaviour of high-voltage 4H-SiC BJTs, and the experimental validation thereof. High voltage silicon BJTs are impractical due to their low current gain which requires a bulky base driver. Emergence of high voltage 4H-SiC vertical NPN BJTs with a tenfold higher gain enables the application of efficient drivers, with ratings close to those of IGBTs. This paper demonstrates the advantages offered by 4H-SiC BJTs by means of wide-scale measurements at 800 V and 10 A in a range of temperatures up to 175°C and adjusted base driver switching rates. The paper shows that the turn-off storage delay in the SiC BJT is two orders of magnitude lower than that of the silicon device. It also shows that the turn-on switching transients of SiC device are by an order of magnitude and the turn-off transients are by two orders of magnitude faster than that of its silicon counterpart, resulting in a tenfold reduction of the switching energy. It also demonstrates the temperature-dependency of switching transients of the silicon BJT, and the relative temperature-invariance of the SiC device's performance. The paper concludes with validation of the transient models for the 4H-SiC NPN BJT, showing that the model is sufficiently accurate for transient switching and loss calculations.**

***Index Terms*—Bipolar Junction Transistor, Temperature, Silicon Carbide, Power Semiconductor Devices, DC Gain**

I. Introduction

SILICON bipolar junction transistors (BJTs) are designed in both lateral and vertical structures. The low DC current gain (h_{FE}) in the high voltage (800 V) silicon vertical BJTs makes them an unattractive choice for power electronics applications due to the need for complex base drivers. Therefore, in the past decade these current-driven devices were largely pushed aside by the voltage-driven devices such as silicon metal-oxide-semiconductor field-effect transistor (MOSFETs) and insulated gate bipolar transistors (IGBTs). The advantages of the latter devices is realized by a gate oxide between gate metallization and the P-type body region, forming a channel. It is now evident that the existence of this gate channel creates reliability challenges [1] especially at higher temperatures [2]. This worsens when silicon carbide (4H-SiC) is used to fabricate the devices [3]. BJTs inherently do not have gate oxide and therefore do not suffer from the oxide reliability issues or reduced channel mobility due to lower carrier concentrations in the cannel [4]. In addition the low current gain (h_{FE}) in silicon power BJTs is recently significantly improved (by at least an order of magnitude) in SiC BJTs [5]. This is due to the wider bandgap and higher critical electric field of the device enabling reduction of dimensions of the base and voltage-blocking drift region. This, in turn, provides higher efficiency in emitter/collector junctions and a higher current gain [6]. Other bipolar devices, i.e. IGBTs, could also be made by SiC [7], although only practical for extremely high voltages. Fabrication of BJTs by 4H-SiC also enables increasing the voltage level to significantly higher values, as the leakage current is reduced and therefore the natural bipolar multiplication of BJT does not occur prematurely [8]. This expands the safe operating area (SOA) which is normally limited by the secondary breakdown [9].

Application of SiC BJTs are already demonstrated in power converters such as the 200 A & 50 kW DC-DC converter assembled solely by SiC BJTs yielding an extremely high efficiency for potential application in electric vehicles. It is shown that each SiC BJT has a current density of over twice that of silicon IGBTs [10]. High voltage ($\geq$800 V) BJTs are also still in demand as deflection transistors in certain special screens [11]. If reverse conduction is not required, such as in boost converters, SiC BJTs have a comparable, if not better, conduction efficiency over unipolar devices [12]. When reverse conduction is required the available reverse conduction path of silicon power MOSFETs via the anti-parallel bipolar body diode is not useful too due to the extremely poor reverse recovery of the body diode. This is even worse in superjunction power MOSFETs. The bipolar reverse recovery deteriorates in higher temperatures by increase of minority carrier lifetimes in silicon. The very low minority carrier lifetime in SiC and smaller temperature-dependency assist in overcoming this challenge in bipolar SiC devices. SiC BJTs also do not exhibit reliability challenges of the gate oxide of SiC MOSFETs and IGBTs in high temperatures [13]. In addition to significant improvement in current gain (h_{FE}) and a smaller base driver, the bipolar structures enable conductivity modulation to reduce the on-state resistance. SiC BJTs are the

Manuscript received November 30, 2018; revised 28 February 2019 and 10 April 2019, accepted 30 May 2019. Date of publication June 2019; date of current version June 2019.

S. Jahdi, M. Hedayati, B. H. Stark and P. H. Mellor are with the Electrical Energy Management Group, Department of Electrical Engineering, University Of Bristol, Bristol BS8 1UB, U.K. (e-mail: saeed.jahdi@bristol.ac.uk; m.hedayati@bristol.ac.uk; Bernard.Stark@bristol.ac.uk; P.H.Mellor@bristol.ac.uk).

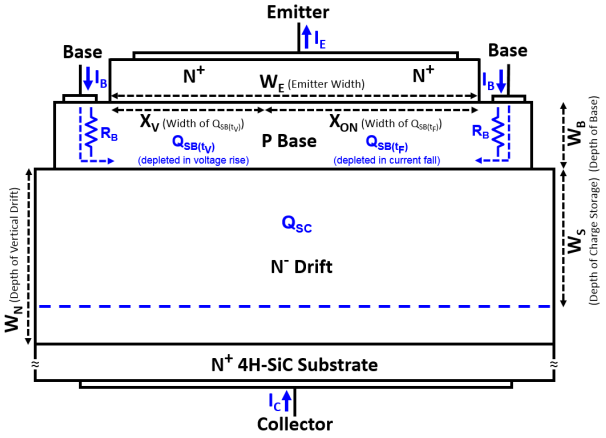

Fig. 1. Cross-section schematic of an epitaxial high voltage ($\geq$ 800 V) vertical NPN 4H-SiC BJT [17].

only wide-bandgap device that has a significant short-circuit capability (up to 20 μs at full voltage) [8]. Therefore, they can be used in applications such as inductive motor drives with short-circuit requirements [8]. SiC BJTs have a high avalanche ruggedness [14] and have square reverse bias safe operating area (RBSOA). The smaller parasitic capacitors due to smaller size of the device also means less ringing at the output [15]. Fig. 1 represents the cross-section structure of such a vertical NPN BJT with main device parameters identified as listed in table I. The high voltage 4H-SiC BJTs are currently only made in NPN structure due to the lack of highly-doped P-type substrates with high conductivity. Similar to other high voltage device structures, it also has a drift region to form the depletion area to enable it sustain high voltages [16].

This paper investigates the performance of 4H-SiC BJTs as opposed to vertical silicon BJTs with analysis of dynamic switching transients seen in experimental measurements in a wide range of temperatures (25°C to 175°C) and base resistances (R_{Base} = 3.75 Ω to 11.75 Ω). Section II discusses the analytical modelings required for understanding of the dynamic transients of power BJTs; section III explains the experimental set-ups; section IV provides the measurements results while section V concludes the paper.

II. Modeling Analysis

To analyse the performance of the device shown in Fig. 1 all the parameters have to be first defined. These are listed in table I to analytically describe the dynamic switching transients of high voltage NPN BJTs. The doping of drift region (N_D in W_N) is at least an order of magnitude lower than the doping of base (N_B in W_B). Likewise, the doping of the emitter region is at least an order of magnitude higher to enhance the emitter injection efficiency and the gain. The minority carrier charge stored in the base is two sections which is $Q_{SB(t_V)}$ removed during the voltage rise section of the turn-off transient and the $Q_{SB(t_F)}$ removed during the current drop section of the turn-off transient. The X_V region is the length of the part of the base which incorporates the $Q_{SB(t_V)}$ minority carrier charge while X_{ON} is the length at which the $Q_{SB(t_F)}$ minority carrier charge is stored during current turn-off.

TABLE I
Nomenclature

Parameter	Symbol	Parameter	Symbol
BJT DC Gain	β (h_{FE})	Collector Stored Charge	Q_{SC}
Diffusion Coefficient	D	Base Stored Charge	Q_{SB}
Charge Storage Width	W_S	Collector Current Density	J_C
Drift Region Width	W_N	Base Current Density	J_B
Base Region Width	W_B	Minority Carrier Lifetime	τ
Emitter Region Width	W_E	Mobility	μ
Base Region Doping	N_B	Temperature	T
Drift Region Doping	N_D	Relative Permittivity	ε

To understand the transient dynamics, the dependencies of key parameters, such as carriers mobility, diffusion coefficient and the minority carriers lifetime must be first discussed.

The temperature dependence (<500 K) of mobility of holes and electrons in silicon and 4H-SiC in low doping is [18]:

$$\mu_n|_{Si} = 1360\left(\frac{T}{300}\right)^{-2.42} \quad (T<500K) \tag{1a}$$

$$\mu_p|_{Si} = 495\left(\frac{T}{300}\right)^{-2.20} \quad (T<500K) \tag{1b}$$

$$\mu_n|_{4H-SiC} = 1140\left(\frac{T}{300}\right)^{-2.70} \quad (T<500K) \tag{1c}$$

$$\mu_p|_{4H-SiC} = 120\left(\frac{T}{300}\right)^{-3.40} \quad (T<500K) \tag{1d}$$

So, the diffusion coefficient reduces with temperature due to the strong inverse temperature-dependance of mobility as:

$$D_n|_{Si} \propto \frac{1}{T^{1.42}} \quad (T<500K) \tag{2a}$$

$$D_p|_{Si} \propto \frac{1}{T^{1.20}} \quad (T<500K) \tag{2b}$$

$$D_n|_{4H-SiC} \propto \frac{1}{T^{1.70}} \quad (T<500K) \tag{2c}$$

$$D_p|_{4H-SiC} \propto \frac{1}{T^{2.40}} \quad (T<500K) \tag{2d}$$

The key dependencies for the minority carrier lifetime of electrons and holes in silicon [19], [20] and 4H-SiC [21], [22] for temperatures below 500 K can be also defined as:

$$\tau_n|_{Si} \propto T^{2.20} \quad (T<500K) \tag{3a}$$

$$\tau_p|_{Si} \propto T^{2.80} \quad (T<500K) \tag{3b}$$

$$\tau_n|_{4H-SiC} \propto T^{1.72} \quad (T<500K) \tag{3c}$$

$$\tau_p|_{4H-SiC} \propto T^{2} \quad (T<500K) \tag{3d}$$

The increase of minority carrier lifetime by temperature increases the recombination periods so it impacts the model's predicted transient times. The minority carriers lifetime of 4H-SiC is about 100 times smaller than silicon, resulting in faster transients with less temperature-dependency as shown in equation 3. The impact of this is discussed in section IV.

The 'Webster Effect', as the increase of collector current beyond the onset of high-level injection (HLI), must also be considered in the model's accuracy. The onset is defined by:

$$J_W = \frac{qD_{nB}N_B}{W_B} \tag{4}$$

Turn-on and turn-off transients models [18], [19] are:

A. Turn-on

At the point of turn-on, the holes injected in the base will be diffused toward emitter and attract the electrons toward the P-body base. The reverse bias of the base-collector junction results in drift of minority carriers (electrons) toward the collector, resulting in onset of conduction. The turn-on transients are divided in to the minority carrier charge build-up phase, the current rise phase and voltage drop phase.

1) Charge Build-up Time: To turn-on the BJT, the base first has to build-up enough minority carrier charge to conduct. The minority carrier charge injected from the emitter requires time to travel through the base to reach the collector. The initial recombination in base will make this period longer and it is exacerbated with thicker base region and increase base doping density. This is called 'transit time'. After this period, enough minority carrier charge is available in the base for turn-on transient. Knowing D_n is the diffusion coefficient, we have:

$$t_{T_{on}} = \frac{{W_B}^2}{2D_n} \tag{5}$$

2) Current Turn-on Time: To demonstrate the time required for current turn-on to complete, the rate of minority carrier charge increase in the base has to be determined by its current density, J_B, as:

$$\frac{\mathrm{d}Q_B}{\mathrm{d}t} = \beta J_B \quad \Rightarrow \quad Q_B = \beta J_B t \tag{6}$$

The base current at turn-on will be in saturation region and therefore the charge in the base Q_B rises without increasing the collector current, which means at this stage the value of the βJ_B can be considered constant [6]. Once reached full on-state current we will have:

$$\frac{J_C}{qv_{sat}} = N_D \tag{7}$$

On the other hand, minority carrier charge stored by the electrons is defined according to the triangular space-charge region in the base as:

$$Q_B = \frac{1}{2}qn_BW_B \tag{8}$$

where n_B accounts for the carrier concentration. Combining the above, the relationship between the rate of increase of collector-emitter current with time can be determined as:

$$J_C = qD_n\frac{\mathrm{d}n}{\mathrm{d}x} = qD_n\frac{n_B}{W_B} = \frac{2D_n\beta J_B}{{W_B}^2}t \tag{9}$$

where J_C is the collector current density. From this the time required for the current turn-on transient is:

$$t_{I_{on}} = \frac{{W_B}^2 J_C}{2D_n\beta J_B} = \frac{{W_B}^2}{2D_n} \tag{10}$$

In-line with the physical expectation, it can be seen from equation 10 that as the base gets wider, the rate of rise of current is reduced. Therefore, for SiC with smaller width of the base, this value should be significantly smaller than silicon devices. Also as is demonstrated by equation 9, should the base current, J_B, to be reduced, it will take linearly-increased time for the collector current to rise. These predictions will be shown to be in-line with measurements in the next sections.

To examine the impact of temperature on the duration of the current turn-on transient, several factors has to be considered. It is expected that reduced mobility of carriers in higher temperature to hinder the turn-on. Looking at equation 10, it can be seen that the width of the base region is independent of temperature and the only temperature-dependent parameter is the diffusion coefficient of electrons in the denominator as:

$$D = \frac{kT}{q}\mu \tag{11}$$

Despite the apparent direct linear dependence of diffusion constant with temperature in 11, it actually reduces with temperature in-line with equation 2 due to significant temperature-dependence of the of mobility. Implementing equation 2 in 11 and subsequently replacing it in equation 10, it becomes clear that by increase of temperature, the duration of current turn-on transient must be increased.

3) Voltage Turn-on Time: During turn-on, first the BJT will take on the nominal current before its voltage drops to the on-state level. As shown, the rate of increase of the current during turn-on depends on the rate at which minority carrier charge is build-up in the base region of BJT, while the rate at which voltage drops depends on the rate at which minority carrier charge in build-up in the drift region. The stored minority carrier charge in collector side of collector-base junction, Q_{SC}, increases resulting in the decrease of the on-state resistance, which subsequently results in reduced voltage drop. The period is defined by the minority carrier charge build-up per collector-current as:

$$t_{V_{on}} = \frac{Q_{SC}}{J_C} = \frac{qN_DW_N + qN_BW_B}{J_C} \tag{12}$$

None of the parameters in the numerator of equation 12 are temperature-dependent. However, J_C is temperature-dependent through temperature dependency of diffusion coefficient, resulting in $t_{V_{on}}$ to increase with temperature. This will be shown to be in agrement with measurement in the next section.

B. Turn-off

During on-state the base and drift region of BJT is flooded with minority carriers. Therefore, at turn-off there will be a period of delay as a result of recombination and extraction of the stored minority carriers which is mainly in the base. This is called the base minority carrier charge storage time. Once this phase is over, then the depletion region can start to form to initiate the voltage rise and current drop phase can follow to complete the turn-off transient.

1) Charge Storage Time: Using the equation 10, the charge stored in the base of the BJT can be written as:

$$Q_{SB} = t_{I_{on}} \beta J_B = \frac{{W_B}^2 J_C}{2D_n} \tag{13}$$

The stored minority carrier charge in the collector region can also be determined by the minority carrier charge from equation 12 as:

$$Q_{SC} = \frac{1}{2} q p_{BC} W_S = \frac{D_p {W_N}^2 {J_C}^2}{4D_n (D_n J_B + D_p J_C)} \tag{14}$$

where the width of stored minority carrier charge section in the drift region of device, measured from the base-collector junction, is:

$$W_S = \frac{D_p W_N J_C}{D_n J_B + D_p J_C} \tag{15}$$

As a result, the total stored minority carrier charge is:

$$Q_S = Q_{SC} + Q_{SB} = J_B t_S \tag{16}$$

and from the stored minority carrier charge, storage time can be derived as:

$$t_{S_{off}} = \frac{J_C}{J_B} \left(\frac{{W_B}^2}{2D_n} + \frac{{W_N}^2}{4D_n} \frac{D_p J_C}{D_n J_B + D_p J_C} \right) \tag{17}$$

Looking at equation 17, it may appear that with increase of base resistance the base current will be reduced which will result in increase of the storage time. However, the base current and collector current are proportionate to each other with h_{FE} (β). On the other hand, the impact of base current can be accounted for in the W_N as the charged region expands further in the drift region as the current increases. This means with decrease of base current as a result of increase of base resistance the minority carrier charge storage area is decreased and therefore the delay period decreases. On the other hand, it is clear that the diffusion coefficient (D_n) has a critical role in determination of storage time. As shown in equation 2, the diffusion coefficients reduce with temperature and therefore the storage time will increase with increase in temperature. The significant dependence of the storage time to dimensions of the base and collector regions (by power of 2) means that reducing the size of the device should reduce the stored charge significantly. As will be seen, 4H-SiC is using this property for achieving a swift transient as oppose to slow response time of the silicon device to the base signal.

2) Voltage Turn-off Time: For the voltage to start to rise at turn-off, minority carrier charge in the depletion region must be removed. The amount of the remaining charge depends on the area of depletion region. This can be shown as:

$$Q_{SD}(t_e) = q N_D W_D(t_e) = 2qD_p \frac{p(W_S)}{W_S} t_e \tag{18}$$

from which the voltage dropped on this region can be written as:

$$V_C(t_e) = \frac{qN_D}{2\varepsilon_s} {W_D}^2(t_e) = \frac{\left(2qD_p \frac{p(W_S)}{W_S} \right)^2 {t_e}^2}{2q\varepsilon_s N_D} \tag{19}$$

from which the time for rise of collector voltage can be written as:

$$t_{V_{off}} = \frac{\sqrt{2q\varepsilon_s N_D V_{CS}}}{2qD_p \frac{p(W_S)}{W_S}} \tag{20}$$

In the equation 20, the diffusion coefficient is the main temperature dependent parameter, which reduces with temperature in-line with equation 2. So the required time for rise of collector voltage has to increase with temperature. This will be confirmed to match the measurements.

3) Current Turn-off Time: The base charge transient rate is:

$$\frac{\mathrm{d}Q_{SB}}{\mathrm{d}t} = \frac{J_C {W_B}^2 L_E}{2D_n} \frac{\mathrm{d}X_{ON}}{\mathrm{d}t} = I_x(X_{ON}) - I_B \tag{21}$$

where $I_x(X_{ON})$ [18], [19] can be written as:

$$I_x(X_{ON}) = \frac{qD_n n_{EB} W_B L_E}{2L_n} = \frac{J_C {W_B}^2 L_E}{2L_n} \tag{22}$$

where X_{ON} is the portion of the base which is still in on-state and the L_E is the length of the emitter region.
The current turn-off time period can be derived by Eq. 21 as:

$$t_{I_{off}} = \frac{W_E - X_V}{\frac{2D_n W_E}{{W_B}^2 \beta} - \frac{D_n}{L_n}} \tag{23}$$

where X_V is the portion of base region which is turned-off by rise of the voltage and the diffusion length is [13]:

$$L_n = \sqrt{D_n \tau_n} \tag{24}$$

Equation 23 shows that $t_{I_{off}}$ is also temperature dependant via the diffusion coefficient and minority carrier lifetime. With increase of temperature the diffusion coefficient reduces as per equation 2 while the carrier lifetimes increases with temperature with almost the same rate as per equation 3. Therefore, the diffusion length is almost temperature invariant. Nevertheless, the reduction of the diffusion coefficient with temperature results in increase of the time required for the current to fully turn-off. This will be in-line with results of experiments. The modeling analysis provided in this section will be used in section IV to understand and explain the experimental measurements and to evaluate the difference of the models applicable to the silicon and 4H-SiC BJTs.

III. Experimental Set-Up

To understand the impact of base resistance and temperature on latest generation of high voltage ($\geq$ 800 V) silicon and 4H-SiC power BJTs, a range of experimental measurements are performed. To this end, power BJTs are connected in a double-pulse arrangement with parameters as described in table II and a dedicated base driver with driver parameters as described in table III to switch the BJTs. They are connected to a high voltage (1200 V) SiC Schottky barrier diode and a 4 mH load inductor. The base resistance of the driving circuitry is changed from 3.75 to 11.75 Ω while the Si/SiC BJT temperature is linearly increased from 25°C to 175°C in steps of 25 degrees. The double-pulse durations are sufficient

to increase the current to 10 A given the size of inductor while the applied voltage to both the silicon and SiC BJT is 800 volts. The wide range of measurements enable accurate estimation of performance of both devices in applications.

TABLE II
MEASUREMENT GA100SBJT12-FR4 BOARD COMPONENTS

Parameter	Symbol	Value
DC Capacitor	C_{DC}	5 mF
De-Coupling Capacitor	C_{HF}	100 nF
Load Inductor	L	4 mH
Voltage	V	800 V
Current	I	10 A
Charging Pulse Length	t_{Q1}	35 μs
Switching Pulse Length	t_{Q2}	8 μs
Gap between Pulses	t_{Qnil}	30 μs
Temperature Range	T	25-175°C
Base Resistance Range	R_{Base}	3.75-11.75 Ω
Estimated Parasitic Inductance	L_{Stray}	60 nH

TABLE III
BJT BASE DRIVER GA03IDDJT30-FR4 PARAMETERS

Parameter	Symbol	Value
Driver Input Supply Voltage	V_{CC}	12 V
Output Peak Base Current	$I_{B,switch}$	4 A
Output On-state Base Current	$I_{B,on\text{-}state}$	0.35 A
Output Base Voltage Rise Time	t_{rise}	21 ns
Output Base Voltage Fall Time	t_{fall}	14 ns
Base Capacitor	C_B	10 nF
Charging Resistor	R_{B1}	1 kΩ
Base Resistor	R_{B2}	3.75 Ω

Fig. 2 shows the circuit for the test rig which is comprised of a high voltage 4 kV ETPS power supply connected to 5 mF DC link capacitors mounted on the test board as in table II. The high voltage transistors are GeneSiC 4H-SiC BJT (1700 V) and Fairchild silicon BJT (800 V) while the load anti-parallel diode is a CREE SiC Schottky diode. When analysing the measurements, one should take into account the difference between the voltage rating of the SiC device (1700 V) with the silicon device (800 V) for the closely-rated current capability of 15-20 A for both devices while the test conditions has been 800 Volts and 10 A. The base driver, as in table III, is connected to the transistors in a common-emitter configuration through a variable base resistor. Measurements are captured via two GW-Instek GDP-100 100 MHz voltage probes and current Rogowski coils connected to a Keysight MSO7104A 1 GHz 4 GSa/s oscilloscope.

To prevent oscillations on the DC link upon switching, a high voltage 100 nF de-coupling capacitor is connected between SBD diode cathode and BJT emitter, immediately in vicinity of DUTs. Fig. 3 shows the test components inside the test rig. The test board is capable of sustaining voltages

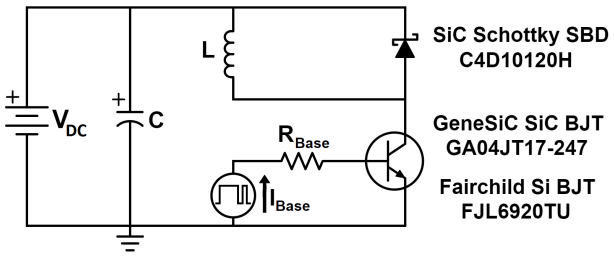

Fig. 2. The devices as DUT in the double-pulse test circuit.

as high as 1.2 kV while the tests has been performed at 800 volts. The stray inductance is minimized by ensuring that the components are as close to each other as possible. The stray inductance of the test board is estimated to be 60 nH. Table IV enlists the main properties of the DUTs and table V enlists the extracted physical parameters [18], [19], [23]–[26].

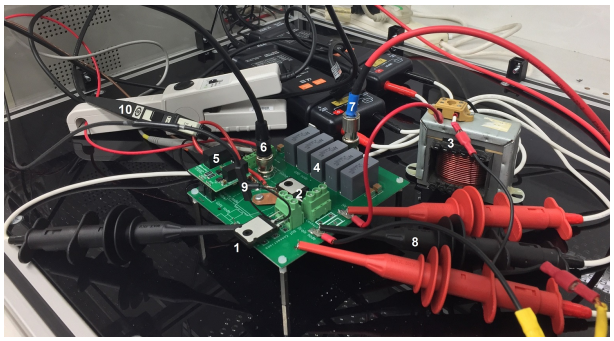

Fig. 3. The test rig components: 1- BJT transistor, 2- Diode, 3- Load Inductor, 4- DC Capacitors, 5- Base Driver, 6- Input Signal, 7- HV supply, 8- Voltage Probes, 9- Rogowski Coil & 10- Current Probe.

TABLE IV
THE HIGH VOLTAGE SILICON AND 4H-SIC NPN BJT AS DUTS

	4H-SiC	Si
Model	GA04JT17-247	FJL6920TU
Manufacturer	GeneSiC	Fairchild
Collector-Emitter Voltage *(V)*	1700	800
Collector Current *(A)*	15	20
Power Dissipation *(W)*	106	200
DC Current Gain - h_{FE} *(-)*	100	8
J-C Thermal Resistance *(°C/W)*	1.41	0.625
B-E Saturation Voltage *(V)*	3.45	1.5

The collector-emitter voltage limit of silicon device is 800 volts and therefore the tests has been limited to this. It must be noted that this is one of the highest voltage levels available for a commercial silicon BJT [27]. The SiC device, on the other hand, can sustain voltages as high as 1700 volts with prospect of emergence of higher voltage SiC devices in the foreseeable future. It can be seen in table IV that despite having larger blocking voltage capability and close current rating, the power dissipation limit for the SiC device is lower than that of the silicon device, which is primarily due to

TABLE V
EXTRACTED DEVICE STRUCTURE PARAMETERS

	4H-SiC	Si
Drift Region Doping (N_D)	$\sim 10^{15}\ cm^{-3}$	$\sim 10^{14}\ cm^{-3}$
Base Region Doping (N_B)	$\sim 5\times 10^{16}\ cm^{-3}$	$\sim 10^{16}\ cm^{-3}$
Drift Region Width (W_N)	$\sim 12\ \mu m$	$\sim 80\ \mu m$
Base Region Width (W_B)	$\sim 5\ \mu m$	$\sim 15\ \mu m$
Relative Permittivity (ε_r)	~ 9.6	~ 11.7
Minority Carrier Lifetime (τ_n)	$\sim 1\ \mu s$	$\sim 100\ \mu s$
N.B.: @ N_A=$10^{15}\ cm^{-3}$ & T= 25°C		

smaller die size and the limited heat transfer between the die and case. Nevertheless, a key advantage of SiC BJTs compared with high voltage (800 V) silicon BJTs is their significantly higher DC gain, typically an order of magnitude higher, primarily due to significant reduction in the width of the base and drift regions enabling a more compact structure, reducing losses in the driver and enhancing the efficiency of the emitter injection. The SiC BJT is more rugged than SiC MOSFETs due to lack of the silicon-oxide gate failure-mode [5] while the high DC gain means the driver's output current is in the same range.

IV. EXPERIMENTAL MEASUREMENTS

Dynamic transients of vertical silicon and SiC BJTs are evaluated by comparison of their switching characteristics. Fig. 4 shows the base and collector current ramp-up at 800 V. Fig. 4(A) shows when the base turns-off, a significant delay exists until the collector current drops and the silicon BJT turns-off. This is about 10 μs at 25°C while with increase of temperature it further increases. The delay for second pulse is shorter as the interval available for carriers to be stored is reduced. On the contrary, Fig. 4(B) shows that for the 4H-SiC BJT both the turn-on and turn-off transients take place almost concurrent with the switching of the base current, indicating the role of significantly smaller drift region, shorter base width and lower minority carrier lifetime in the SiC device. This is a promising feature for application in higher frequency.

Fig. 5 shows the trends of turn-off storage time with base resistances and temperatures. It is seen that the storage time in silicon BJT is averaging 10 μs thereabouts, hindering its utilization in high frequency applications while the values of delay in SiC are much lower as indicated in the legend. This indication has been done in all figures where measurements values for SiC are not easily distinguishable due to the significant differences with silicon. The delay further increases with increase of temperature due to increase in minority carrier lifetime at higher temperatures. It is also shown that storage time is reducing with increased base resistance due to the reduced width of storage region. The lower storage time in SiC was expected from equation 17 where it is seen that as the width of the base and drift region reduces the storage time will reduce. Therefore, the reduction of storage time in SiC is significantly rely upon smaller dimensions of the die.

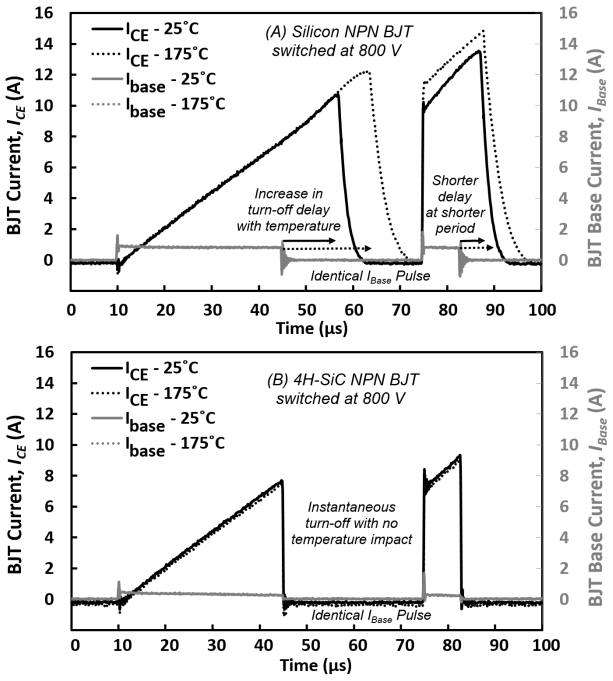

Fig. 4. The base and collector current in the double-pulse test showing a significant temperature-dependent turn-off storage time in (A) silicon BJT while the delay in (B) SiC device is negligible. Note that the base current supplied for all cases is identical to enable for a fair comparison.

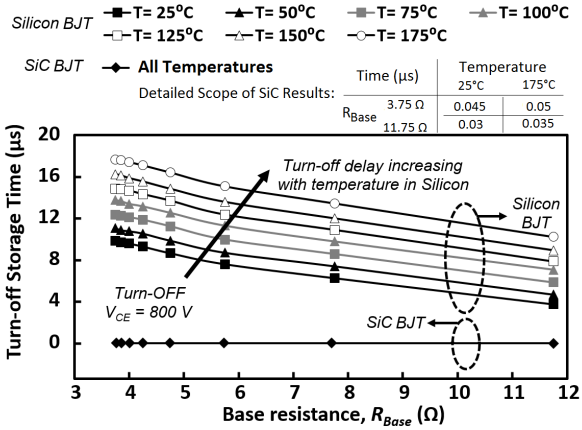

Fig. 5. The turn-off storage time in silicon BJT switched at 800 volts is significant and is temperature-dependent, while in comparison the storage time in 4H-SiC BJT is negligible.

To evaluate the switching performances, the time it takes for each device to complete its transient is measured by calculation of the period it takes to reach the expected value, excluding the impact of turn-off delay period. In-line with the analysis of section II, each switching is separated into two sections: the minority carrier charge displacement and the transients phase described in terms of current and voltage switching times. The initial minority carrier charge build-up phase is small for both devices, however the minority carrier charge recombination phase (turn-off delay period) is substantial, especially for the silicon device due to the higher minority carrier lifetime of silicon by two orders of magnitude. Fig. 5 has plotted this delay. Fig. 6 & 7 indicate the transient

time for the current/voltage to reach the same level. The impact of turn-off delay on increase of the current is not considered to enable a fair comparison between transient times.

Fig. 6(A) shows the time it takes for the current to ramp-up to on-state when switched at 800 V and 10 A. It is seen that the turn-on time for current is higher for silicon BJT compared with the SiC device and the transient period increases as the base resistance increases, which results in less base charge supplied to the device to turn-on. The current transient is also temperature dependent in silicon device, with a bolder impact as the base current in the device is reduced. In contrary, the current turn-on phase for the SiC is short without significant temperature dependence. This was demonstrated by equation 9 which indicates that the increase of current with time depends on the base width by power of two, which is smaller for SiC, hence resulting in a faster current transient.

Fig. 6(B) shows the same characteristics for the turn-off transient. It can be seen that the turn-off transient for current is significantly longer that its turn-on by an order of magnitude, which was expected due to storage of carriers and subsequent extraction and recombination in the base and drift regions of device, while in the SiC device this is significantly shorter due to the low minority carrier lifetime and smaller dimensions of the die. This is in-line with the trend expected by equation 23 where the dependence of current turn-off time with base width with power two means the devices with thicker base region would have a slower current transient time.

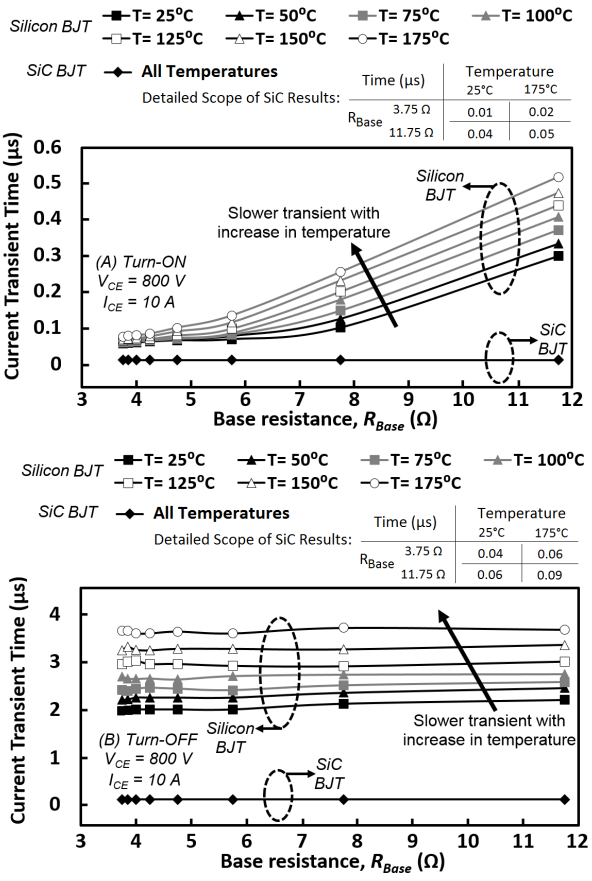

Fig. 6. The current transient time for silicon & 4H-SiC NPN BJT at 800 V at (A) turn-on & (B) turn-off, in a range of R_{Base} and temperatures.

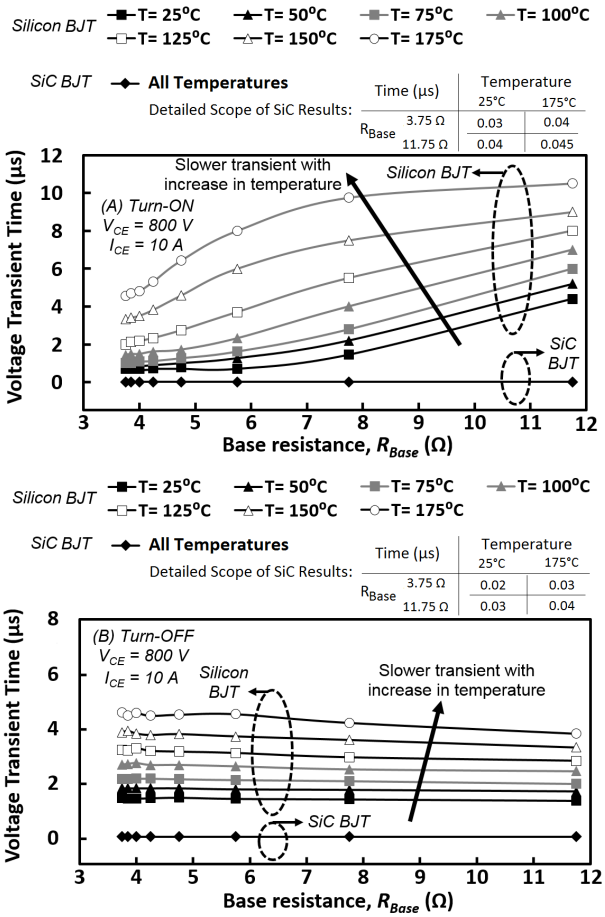

Fig. 7. The voltage transient time for silicon & 4H-SiC NPN BJT at 800 V at (A) turn-on & (B) turn-off, in a range of R_{Base} and temperatures.

Fig. 7(A) shows the period voltage takes to drop in the turn-on transient. It is seen that by increase of base resistance the time required for voltage drop increases as it takes longer to fill the depletion region by carriers and consequently reduce the voltage drop across the BJT. Also by increasing the temperature the voltage drop transient at turn-on prolongs as the diffusion constant of carriers reduces with increase in temperature. This is in-line with expectations by equation 12 where the turn-on time of the voltage is seen to increase as the charge stored in collector side is higher (which means a higher negative base current is required for extraction which requires a lower base resistance) and it increases with temperature as the diffusion constant in the denominator reduces.

Fig. 7(B) shows the period voltage takes to rise at turn-off. As seen, the dependence is largely on temperature than the base resistance. At higher temperatures, due to higher carrier lifetime in silicon and reduced mobility, it takes longer for the carriers to leave the drift region to enable the space-charge to form. Hence, the voltage rise transient interval is longer in higher temperatures which was expected from equation 20 due to the impact of diffusion constant. In SiC device, the smaller die size enables faster temperature-invariant transient.

Fig. 6 and 7 are derived based on the switching performance of vertical silicon and SiC BJT which is demonstrated in Fig. 8 and 9. These figure indicate the current and voltage turn-on and turn-off transients for both silicon and SiC devices in the same

graph to enable a fair comparison between the switchings.

Fig. 8(A) shows the current turn-on transient for both the silicon and SiC BJTs. The turn-on current in SiC device is slightly faster although it is prone to more ringing compared with the silicon device. However, the difference in the collapse of voltage in the two devices is much more evident. As seen in Fig. 8(B), the voltage drop in the silicon device takes much longer than the SiC device, which is due to the significant difference in the widths of the drift regions. This is expected in line with equation 20. It should be noted that the on-state current in the silicon device is higher than the SiC device due to the turn-off storage delay resulting in prolonged period of load current ramp-up. This was demonstrated in Fig. 4.

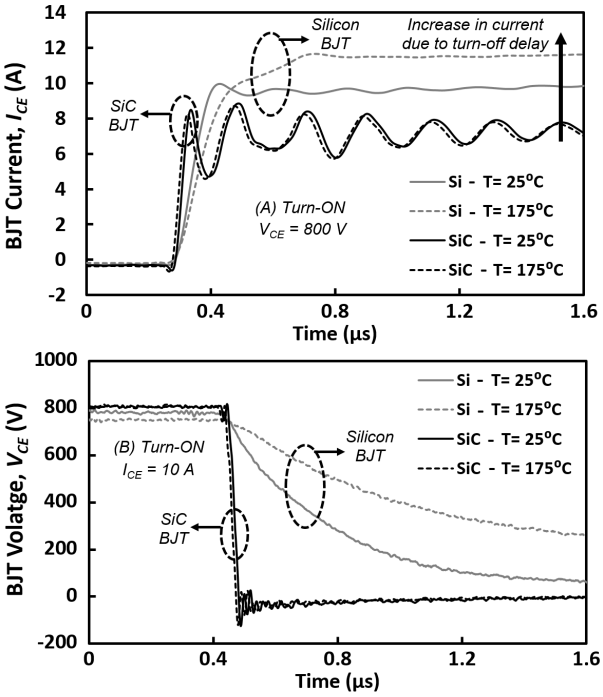

Fig. 8. Turn-on transient of silicon and 4H-SiC BJT switched at 800 V with R_{Base} of 3.75 Ω for (A) current & (B) voltage at 25°C and 175°C.

Fig. 9 shows the turn-off transients. Fig. 9(A) shows the current transient, where the silicon device is much slower compared with the SiC device. The on-state current is higher for the silicon device due to the impact of turn-off delay. At increased temperature, the increased carrier lifetime and lower mobility results in prolonged periods of extraction and recombination of minority carriers, which results in slower switching commutation. As the carriers are removed slower, the formation of space-charge in the drift region will also take longer, resulting in lower *dV/dt* and higher losses. In case of the SiC device, it can be seen that the transient is faster as minority carrier lifetime is lower and die size is smaller.

An important phenomenon that impacts the transient durations of the devices is the high-level injection (HLI). The high-injection effect has to be considered in the forward biased base-emitter junction. The effect of high injection is more noticeable in the base region as its doping is typically an order of magnitude lower than the emitter region. Injection of electrons in the base from the emitter side increase the carrier concentration which would reduce the injection efficiency and the DC gain. As the doping in the base of the SiC BJT is higher than that of the silicon device (typically by an order of magnitude), the onset of reduction of gain in SiC device occurs at higher currents which is closer to the current rating of the device and hence an optimized performance. Therefore, HLI is seen to have a considerably less impact for the same current conduction level on SiC devices as demonstrated in Fig. 9 with the sharp rate of current transient [28]–[32].

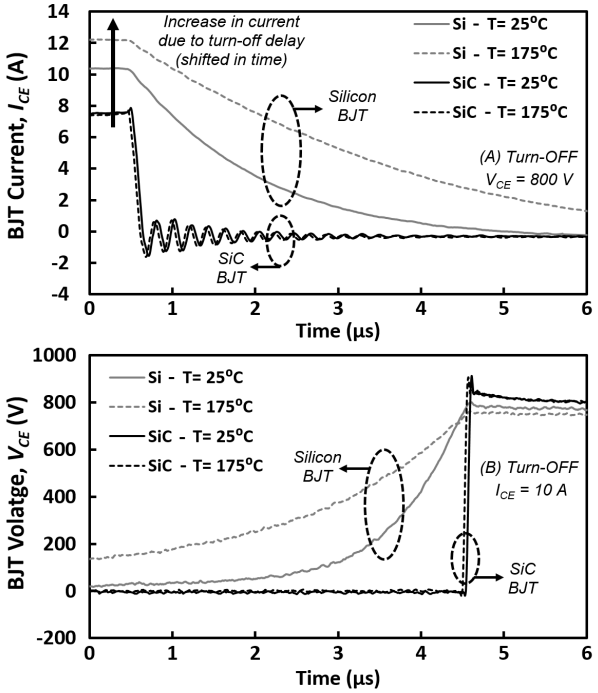

Fig. 9. Turn-off transient of silicon and 4H-SiC BJT switched at 800 V with R_{Base} of 3.75 Ω for (A) current & (B) voltage at 25°C and 175°C.

It can be seen in Fig. 8 & 9 that the performance of the silicon device is significantly dependant on temperature, while the switching transients of the SiC BJT are relatively invariant of temperature. This is due to several different factors such as:

- The minority carrier lifetime in SiC is about two orders of magnitude less than that of the silicon. As a result, the recombination phase in turn-off transients of the SiC is very fast. Equation 3 had also shown that the impact of temperature on minority carrier lifetime of SiC is less.
- The wide-bandgap of SiC means the thermal energy required by carriers to jump the energy bands is higher. Therefore, increased scattering and Auger recombination by generation of additional carriers is limited.
- The higher critical electric field of SiC also means that the device dimensions are smaller. Therefore, all parasitic elements including the junction capacitors are minimized. This increases the gain which reduces the base current and results in more damped oscillations as in Fig. 11.

The aforementioned features make the SiC BJT an attractive choice in high temperature applications. Fig. 8 & 9 show very stable performance for the SiC device in a large range of temperatures in contrary to the silicon device. SiC bipolar devices have little temperature-invariant residual charge as

is reflected here in terms of much shorter turn-off charge storage delay. This is due to the significantly lower minority carrier lifetime in SiC and its less temperature dependency. Accurate estimation of minority carrier lifetime especially in high temperature is challenging as many parameters influence it. This impacts the accuracy of the models. SiC BJTs normally exhibit slightly positive temperature-coefficient (PTC) but thanks to the wide-bandgap of SiC it can even be made negative (NTC) with careful fabrication, i.e. increase in junction temperature will activate more acceptor dopants by ionization than thermally excited generation of carriers in the wide bandgap. This is done by partial ionization of Aluminium dopants in the base at low temperatures [22] and increase in concentration of holes in the base at higher temperatures, resulting in reduced emitter efficiency [22]. This makes the SiC BJTs suitable for parallel connection in high-currents. The fast switching transients in SiC result in lower losses compared with silicon BJT. The thermal conductivity of the SiC is also more than double of the silicon, which means the resultant switching energy is dissipated more effectively. Together, these mean that the thermal stress on the SiC device junction is lower than that of the silicon device under the same conditions.

Fig. 10 and 11 show the turn-on and turn-off base current of both devices when switched at 800 V and 10 A. The turn-on current spike, while having the same duration, is 3.5 A for the silicon device while it is 2.5 A for the SiC device. This peak is followed by reduced ongoing steady-state current. The initial spike supplies enough current to charge the junction parasitic capacitances and supply enough carriers to the base region to initiate turn-on. Subsequently, the base current is reduced to steady-state level to maintain the BJT in on-state while keeping the driver losses low. The parasitic capacitances in the SiC BJT are smaller than that of the silicon device, so the initial peak is reduced by 1 A. The on-state current in SiC is also lower due to higher DC gain. These mean that the SiC device can be drived by a cheaper and smaller driver, with higher driver efficiency. It is seen that in neither case the base current supplied by the driver is affected by the temperature of BJTs as parasitic capacitances are temperature-invariant. Fig. 11 shows the base current for turn-off transients. As seen in Fig. 11(A), at turn-off the large charged base capacitors are coupled with stray inductances in the silicon device and discharge significant current peak of -2 A with coupled with large oscillations. The peak discharge current in SiC BJT base is only -1 A with a damped ringing due to the smaller parasitic capacitors as a result of the smaller dimensions of the SiC die.

Fig. 12 demonstrates the switching energy of the silicon and 4H-SiC devices at (A) turn-on and (B) turn-off in the spectrum of temperatures and chosen base resistances. The switching energy is derived by taking the integration of transient power (VI) over the time-span of each switching event. It can be seen that the switching energy of the 4H-SiC BJT in all cases is much smaller than that of the silicon device, in range of 100s of μJ. It can also be seen that the due to the increase of transient times with temperature, in both turn-on and turn-off the transient switching energy are increased with temperature. As was expected from Fig. 6(B) and Fig. 7(B), the impact of the base resistance on turn-off switching energy is small since

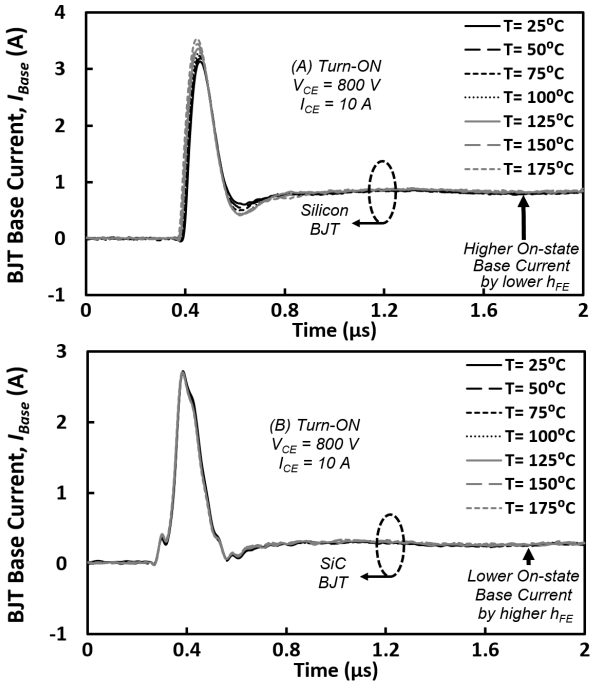

Fig. 10. Base current at turn-on of (A) silicon and (B) 4H-SiC NPN BJT in a range of temperatures from 25°C to 175°C.

the turn-off transient is less dependant on the base current. On the contrary, Fig. 6(A) and Fig. 7(A) show that the current and voltage transient times at turn-on increase with base resistance, so Fig. 12(A) indicates an increase in switching energy.

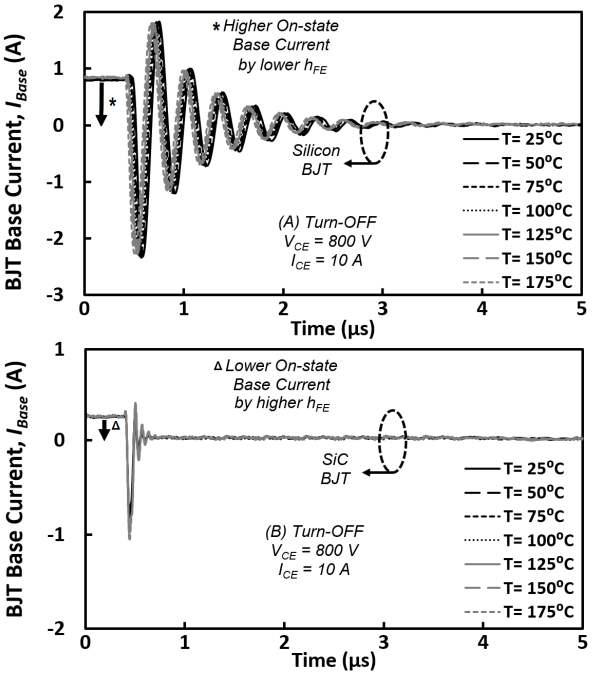

Fig. 11. Base current at turn-off (A) silicon and (B) 4H-SiC NPN BJT in a range of temperatures from 25°C to 175°C.

Parameters listed in table IV & V are implemented in the models of section III to evaluate the performance of the silicon and 4H-SiC NPN BJTs, with comparison to the measurement

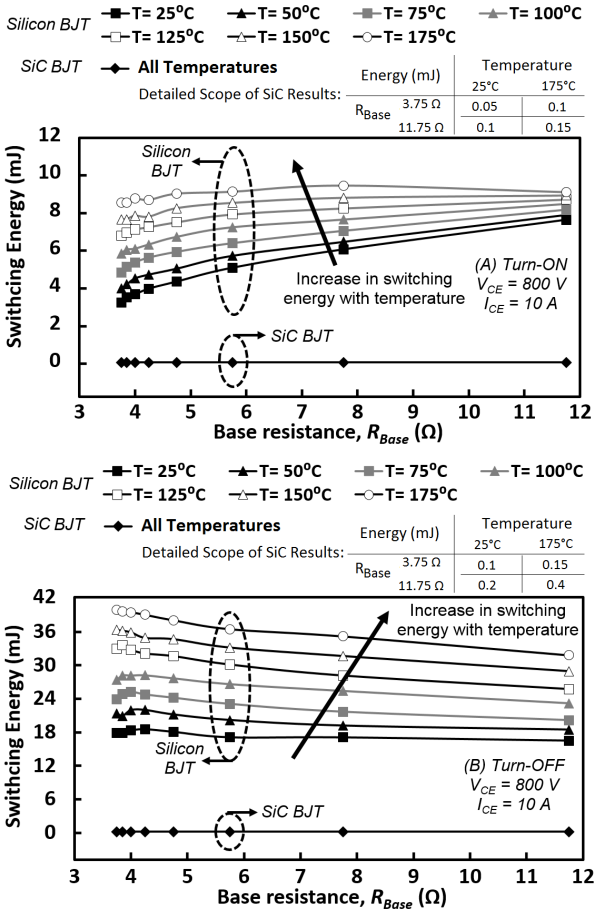

Fig. 12. Switching energy of silicon and 4H-SiC BJT at (A) turn-on and (B) turn-off transient in a wide range of R_{Base} and temperatures.

TABLE VI
MODELS & MEASUREMENTS OF SWITCHING TRANSIENT DURATIONS OF SI & 4H-SIC NPN BJT AT T = 25°C WITH R_{Base} = 3.75 Ω

	Model		Measurement	
	Si	SiC	Si	SiC
Turn-on charge build-up ($t_{T_{on}}$)	∼50 ns	∼8 ns	40 ns	10 ns
Turn-on current transient ($t_{I_{on}}$)	∼50 ns	∼8 ns	54 ns	10 ns
Turn-on voltage transient ($t_{V_{on}}$)	∼200 ns	∼30 ns	342 ns	28 ns
Turn-off charge storage ($t_{S_{off}}$)	∼2200 ns	∼85 ns	9500 ns	45 ns
Turn-off current transient ($t_{I_{off}}$)	∼1400 ns	∼65 ns	2140 ns	39 ns
Turn-off voltage transient ($t_{V_{off}}$)	∼900 ns	∼20 ns	1420 ns	18 ns

results in table VI. As expected by equation 5 and 10, the initial minority carrier charge built-up and turn-on current transient times are similar. The overall predictions of the transients match reasonably well with experiment, especially for the case of SiC device, although the estimation for the turn-off minority carrier charge storage transient indicates discrepancy with measurement. This can be accounted for by the fact that the complexities of finite element approaches [32] are removed from the model as it is aimed for industrial electronics applications rather than device fabrication. The input parameters are also not necessarily constant such as the graded junction dopings and some dynamically change such as the base stored charge and the minority carrier lifetime, especially under influence of high-level injection (HLI). Minority carrier lifetime particularly impacts the accuracy of calculation of turn-off delay time. Nevertheless both the measurements and model output confirm that the 4H-SiC BJT has superior performance with a practical application outlook.

V. CONCLUSION

A comprehensive range of dynamic transient measurements are presented in this paper, along with validation of an analytical model for the switchings of high voltage silicon and 4H-SiC NPN BJTs. Measurements performed at 800 volts and 10 A with temperatures up to 175°C indicate that the 4H-SiC device outperforms the silicon device by a significant margin. As shown experimentally, the voltage and current transient times in 4H-SiC are at least an order of magnitude shorter than that of the silicon device. This the improved performance in dynamic transients of the 4H-SiC device yields a much lower switching energy compared with that of the silicon device with smaller base current. The turn-off delay time in 4H-SiC device is much lower while the switching transients are distinctly temperature-invariant compared with silicon. These translate into higher frequency switching with smaller driver for size-reduction of passive and cooling ancillaries, enabling compact applications. The turn-on and turn-off switching models are validated with measurements and indicate reasonable output for both the silicon and 4H-SiC NPN power BJTs.

REFERENCES

[1] L. Liao, "New proportional base drive technique for sic bipolar junction transistor," *IEEE Trans. on Pow. Elec.*, vol. 32, no. 6, p. 4600, Jun. 2017.

[2] J. Biela and et al., "Sic versus si; evaluation of potentials for performance improvement of inverter by sic power semiconductors," *IEEE Trans. on Industrial Electronics*, vol. 58, no. 7, p. 2872, Jul. 2011.

[3] H. Sarnago and et al., "A comparative evaluation of sic power devices for high-performance domestic induction heating," *IEEE Transactions on Industrial Electronics*, vol. 62, no. 8, pp. 4795–4804, Aug. 2015.

[4] T. Funaki, "Power conversion with sic device at high ambient temperatures," *IEEE Trans. Pow. Ele.*, vol. 22, no. 4, p. 1321, Jul. 2007.

[5] R. Singh, "Fulfilling the promise of high-temperature operation with silicon carbide devices: Eliminating bulky thermal-management systems with sjts," *IEEE Power Elect. Mag.*, vol. 2, no. 1, pp. 27–35, Mar. 2015.

[6] S. M. Sze and et al., "Physics of semiconductor devices," *Wiley-Interscience*, 2007, 3rd Edition.

[7] A. Pozo and et al., "Improved proportional base driver for sic bjts," *IEEE Transactions on Transportation Electrification*, 2018.

[8] D. Sadik, "Short-circuit protection circuits for sic power transistors," *IEEE Trans. Indu. Elec.*, vol. 63, no. 4, p. 1995, Apr. 2016.

[9] S. Sundaresan and et al., "10 kv sic bjts; static, switching and reliability characteristics," in *Symp. Power Devices (ISPSD)*, p. 303, May. 2013.

[10] G. Calderon-Lopez, "Evaluation of sic bjts for high-power dc converter," *IEEE Trans.s Pow. Elec.*, vol. 29, no. 5, p. 2474, May. 2014.

[11] I. Oh, "A new base driving technique of a high voltage bjt for the horizontal deflection output using a crt," in *IEEE Conf. on ASICs (APASIC)*, pp. 67–74, Aug. 1999.

[12] J. Rabkowski and et al., "Parallel-operation of discrete sic bjts in a 6 kw/250 khz dc/dc boost converter," *IEEE Trans. on Pow. Elec.*, vol. 29, no. 5, pp. 2482–2491, May. 2014.

[13] T. Gachovska, "Modeling, simulation, and validation of a power sic bjt," *IEEE Trans. on Power Electronics*, vol. 27, no. 10, p. 4338, Oct. 2012.

[14] Y. Gao and et al., "Comparison of static and switching characteristics of 1200 v 4h-sic bjt and 1200 v si-igbt," *IEEE Transactions on Industry Applications*, vol. 44, no. 3, pp. 887–893, May. 2008.

[15] M. Nawaz, "Static and dynamic characterization of high power sic bjt modules," *IEEE Trans. Indu. Appl.*, vol. 52, no. 6, p. 4990, Nov. 2016.

[16] V. Niemela and et al., "Sic bjt minimizes losses in alternative energy applications," in *IEEE Energytech*, May. 2013.
[17] S. Sundaresan and et al., "Static and switching characteristics of 1200 v sic junction transistors with on-chip integrated schottky rectifiers," in *IEEE Power Semiconductor Devices (ISPSD)*, pp. 249–252, Jun. 2014.
[18] Baliga, "Fundamnetal of power semiconductor device," *Springer*, 2019.
[19] J. Lutz and et al., *Semiconductor Power Devices: Physics, Characteristics, Reliability*, 2nd ed. Springer Int. Publish., 2018.
[20] Y. Gerstenmaief, "A study on the variation of carrier lifetime with temperature in bipolar silicon devices and its influence on device operation," in *Int. Symp. Power Semic. Devices*, p. 271, May. 1994.
[21] A. Udal, "Investigation of charge carrier lifetime temperature dependence in 4h-sic diodes," *Mater. Sci. Forum*, vol. 556, p. 375, 2007.
[22] X. Li and et al., "On the temperature coefficient of 4h-sic bjt current gain," *Solid-State Electronics*, vol. 47, no. 2, pp. 233–239, 2003.
[23] S. G. Sundaresan and et al., "Characterization of the stability of current gain and avalanche-mode operation of 4h-sic bjts," *IEEE Transactions on Electron Devices*, vol. 59, no. 10, pp. 2795–2802, Oct. 2012.
[24] S. G. Sundaresan and et al., "Rapidly maturing sic junction transistors featuring current gain 130, blocking voltages up to 2700 v and stable long-term operation," *Materials Science Forum*, vol. 778, p. 1001, 2014.
[25] S. G. Sundaresan and et al., "Improvement of current gain stability of sic junction transistors," *Materials Science Forum*, vol. 821, p. 822, 2015.
[26] R. Singh, "1200v sic superjunction trans with current gain 88 ultrafast switching capability," *Mater. Sci. Forum*, vol. 717, p. 1127, 2012.
[27] X. Xu and et al., "Performance evaluation of sic mosfet/bjt/schottky diode in pfc," in *IEEE Applied Power Elec.*, p. 1268, Feb. 2007.
[28] P. Ivanov, "Temperature dependence of current gain in power 4h-sic npn bjts," *IEEE Trans. Elec. Dev.*, vol. 53, no. 5, p. 1245, May. 2006.
[29] Y. Lei, "Influence of base carrier lifetime on the characteristics of 4h-sic bjts," *Superlattices and Microstructures*, vol. 102, no. 2, p. 127, 2017.
[30] E. Danielsson and et al., "Extrinsic base design of sic bipolar transistors," *Materials Science Forum*, vol. 457-460, pp. 1117–1120, 2004.
[31] B. Buono and et al., "Modeling and characterization of current gain versus temperature in 4h-sic power bjts," *IEEE Trans. on Elect. Devi.*, vol. 57, no. 3, pp. 704–711, Mar. 2010.
[32] B. Buono, "Influence of emitter width & emitter-base distance on current gain in 4h-sic bjt," *IEEE Trans. Elec. Dev.*, vol. 57, no. 10, Oct. 2010.

Saeed Jahdi (S'10 M'16) has received the degrees of BSc in Electrical Power Engineering from Iran University of Science and Technology, MSc with Distinction in Power Systems from City University London, and PhD in Power Electronics from the University of Warwick, UK. He was with the HVDC Center of Excellence of General Electric, GE Grid Solutions in Stafford, UK and is currently Assistant Professor of power electronics in Electrical Energy Management Group of University of Bristol. His current research interest includes wide bandgap power semiconductor devices in power electronics. Dr Jahdi is a Chartered Engineer in the UK.

Mohammad Hedayati received the M.E. degree in power systems and the Ph.D. degree in power electronics from the Indian Institute of Science, Bangalore, India, in 2010 and 2016, respectively. He is currently a Research Associate with the Electrical Energy Management Group of University Of Bristol, Bristol, U.K. His research interests include hybrid dc circuit breaker (CB), power electronics, wide-band gap devices, active gate driving, and high-power converters.

Bernard H. Stark received the M.S. degree in electrical engineering from the Swiss Federal Institute of Technology (ETH), Zurich, in 1995 and the Ph.D. degree in engineering from Cambridge University, U.K., in 2000. He spent time as a Junior Research Fellow at St. Hugh's College, Oxford, U.K., and as a member of the Control and Power Group, Imperial College, London, U.K. He is currently Professor of Electrical and Electronic Engineering at the University of Bristol, and a member of the Electrical Energy Management Research Group. His research interests include renewable power sources and power electronics.

Phil H. Mellor received the B.Eng. and Ph.D. degrees in electrical engineering from the Department of Electrical Engineering, University of Liverpool, U.K., in 1978 and 1981, respectively. He is currently a Professor of Electrical Engineering with the Department of Electrical and Electronic Engineering, University of Bristol, U.K. Prior to this, he held academic posts at the University of Liverpool from 1986 to 1990 and the University of Sheffield from 1990 to 2000. His current research interests include high-efficiency electric drives and actuation and generation systems for application in more electric aircraft and hybrid electric vehicles.